# Resolving amorphous solid-liquid interfaces by atomic force microscopy

Kristen M. Burson, Leonard Gura, Burkhard Kell, Christin Büchner, Adrian L. Lewandowski, Markus Heyde,[a] and Hans-Joachim Freund
*Fritz-Haber-Institut der Max-Planck-Gesellschaft, Faradayweg 4-6, 14195 Berlin, Germany*

(Received 22 March 2016; accepted 22 April 2016; published online 16 May 2016)

Recent advancements in liquid atomic force microscopy make it an ideal technique for probing the structure of solid-liquid interfaces. Here, we present a structural study of a two-dimensional amorphous silica bilayer immersed in an aqueous solution utilizing liquid atomic force microscopy with sub-nanometer resolution. Structures show good agreement with atomically resolved ultra-high vacuum scanning tunneling microscopy images obtained on the same sample system, owing to the structural stability of the silica bilayer and the imaging clarity from the two-dimensional sample system. Pair distance histograms of ring center positions are utilized to develop quantitative metrics for structural comparison, and the physical origin of pair distance histogram peaks is addressed by direct assessment of real space structures. *Published by AIP Publishing.*
[http://dx.doi.org/10.1063/1.4949556]

Solid-liquid interfaces play an important role in many natural and industrial processes, including electrochemistry, heterogeneous catalysis, energy storage technologies, and biological processes. Stern layers and solvation mechanisms are still debated even though both are textbook classics.[1] Surface structure investigations provide the key to understanding—and tailoring—the processes which occur at complex solid-liquid interfaces. With the growth in research on nanotechnology and energy storage technologies, the necessity for clear, real-space nanostructure mapping under application-oriented conditions is central.

Surface science has been traditionally focused on studies in ultra-high vacuum (UHV). However, with such powerful and versatile tools as atomic force microscopy (AFM), the determination of real-space surface structures is not limited to ideal vacuum environments. As early as 1993, Ohnesorge and Binnig imaged the $(10\bar{1}4)$ surface of calcite in water with true atomic resolution.[2] Two years later, in 1995, true atomic resolution on the $7 \times 7$ reconstruction of the Si(111) surface in UHV was reported.[3] Despite the early success of Ohnesorge and Binnig in attaining atomic resolution in liquids, the attention of the high-resolution AFM research community over the past 20 years has largely been focused on instrumental developments, image contrast, and material systems under well-defined UHV environments.[4,5] Although under-utilized for high-resolution structural studies to date, liquid-AFM presents a promising route for structural assessment of materials in environments more akin to those environments necessary for realistic application conditions.

High-resolution imaging in liquids has required simultaneously developing the instrumentation and imaging technique alongside sample development. Significant progress has been made in the area of instrumentation development. Photo-thermal excitation of the cantilever has improved the stability;[6] imaging in salt solutions can minimize long range electrostatic contributions and lead to stable tip hydration structures;[7–9] high-frequency cantilevers compensate for the drop in resonance frequency introduced by the liquid environment; liquid cells counter liquid evaporation;[10,11] and optimal cantilever preparation approaches have been explored.[12] Nonetheless, the number of different sample systems which have been imaged with atomic resolution in liquids remains limited.[13–19] High-resolution scanning probe microscopy can be optimally attained on atomically flat materials. Most of the atomic contrast results from the interaction of the front-most tip atom with the underlying sample surface (Figure 1(a)). For materials with highly corrugated surface structures, multiple tip atoms are contributing and produce convoluted images[20] as shown schematically in Figure 1(b). As such, much of the high-resolution liquid-AFM data has been attained on single crystals and cleavable materials (e.g., calcite, graphite, and mica). Often, the identification of defect structures allows one to distinguish lattice resolution from true atomic resolution for crystalline materials.[21] In this context, an atomically flat 2D amorphous material is an ideal playground to test the capabilities of high-resolution liquid-AFM. The atomically flat surface circumvents tip convolution challenges, and the amorphous structures address the challenge of distinguishing between lattice resolution and true atomic resolution.

Both for measurements and applications, the amorphous silica bilayer is a unique sample system. This 2D material is a wide band-gap insulator and contributes to the growing class of 2D materials.[22–24] It is a promising candidate for inclusion in heterostructures of 2D materials for tailored nanoelectronics. Amorphous bilayer silica has a completely saturated bonding structure, without dangling bonds. In contrast to many oxides,[25,26] this film system has been found to be exceptionally stable against hydroxylation,[27] providing a chemical stability optimized for liquid and ambient scanning probe microscopy measurements. Here, we present a study of the amorphous silica bilayer structure in water. Using this ideal sample system, we find qualitative and quantitative agreement between high-resolution liquid-AFM measurements and atomically resolved low-temperature UHV scanning tunneling microscopy (LT-UHV-STM) measurements of the silica

[a]Author to whom correspondence should be addressed. Electronic mail: heyde@fhi-berlin.mpg.de

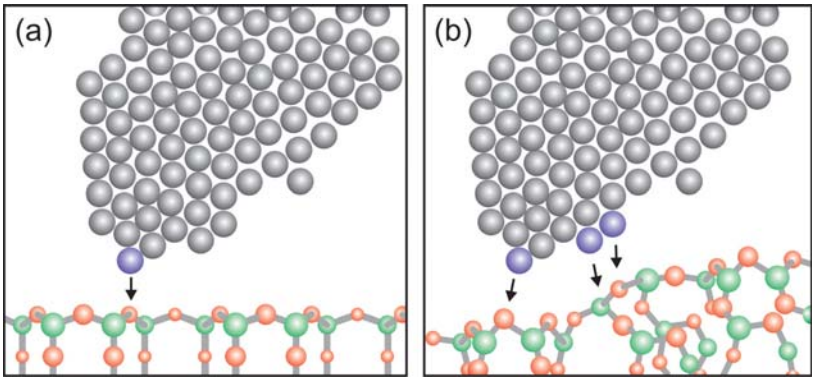


FIG. 1. Schematic diagrams for tip interactions with (a) a 2D film and (b) a 3D material.

bilayer interface structure. Characteristic metrics of medium-range order are identified, and their physical origin is interpreted.

Bilayer silica films were grown in UHV on Ru(0001) single crystals. First, the Ru(0001) crystals are cleaned with cycles of Ar + ion sputtering, UHV annealing to 1523 K, and annealing to 1173 K under an oxygen pressure of $2 \times 10^{-6}$ mbar. Low energy electron diffraction (LEED), Auger electron spectroscopy (AES), and STM were used to control for cleanliness prior to film growth. Well-defined bilayer $SiO_2$ structures were grown by evaporating silicon onto pre-oxidized 3O-$(2 \times 2)$/Ru(0001) at sample temperatures $\leq$300 K and subsequently annealing to $\approx$1200 K in the presence of $2 \times 10^{-6}$ mbar $O_2$. Finally, the samples were cooled down in the oxygen environment. Sample preparation yields either vitreous or crystalline configurations; the coverage and the rate of cooling may impact the final structure.[28,29] Coverage is expressed in terms of monolayers (MLs), where 2 MLs are equivalent to a fully closed bilayer. We observe greater crystallinity with higher coverages (1.9–2.0 MLs), while coverages between 1.5–1.8 MLs yield amorphous domains. Film quality of the sample preparation was checked with LEED, AES, and STM. For the STM measurements, a custom-built, low temperature UHV-STM setup with a tuning fork sensor device was used.[30,31] Images were acquired at T = 5 K. Following this initial characterization in UHV, the sample was rapidly transferred from UHV through air to the liquid environment. An aqueous solution of 400 mM NaCl, prepared with 99.9% purity NaCl and biological grade purity $H_2O$, was used for the liquid environment. It has been found empirically that using a salt solution promotes the imaging resolution.[8,9] The liquid-AFM measurements were performed using a Cypher Environmental Cell with photo-thermal excitation in the amplitude modulation mode. Arrow ultra high frequency cantilevers (f = 700–2000 kHz, k = 25 N/m) were plasma cleaned prior to use (30 W, 5 min). The cantilever and the sample surface were immersed into approximately 80–100 $\mu$l of solution.

In order to verify successful transfer from UHV to liquids, and to assess potential structural changes to the silica bilayer film, LT-UHV-STM and liquid-AFM images from 30 to 200 nm scan ranges are compared. No apparent distortion or degradation of the overall sample structure was observed based on topographic images. Fractional film coverages of less than two full MLs give rise to holes in the silica film structure which expose regions of ML silica coverage and of the Ru(0001) substrate.[32] In the LT-UHV-STM measurements, a density of $4.0 \times 10^{-3}$ holes/nm$^2$ was observed on a 1.7 ML silica sample in comparison to $4.2 \times 10^{-3}$ holes/nm$^2$ derived from the liquid-AFM data for the same sample. Several individual sample spots have been characterized. Overall this provides a quantitative agreement in the hole density as well as their sizes. These measurements indicate a successful sample transfer from UHV to liquids and confirm the stability of the sample structure at nanometer length scale.

On the atomic scale, silica bilayers are composed of a network of connected $SiO_4$ tetrahedra with ring structures in the top plane of the bilayer mirrored in the lower plane. The two planes are connected by Si-O-Si bonds. The structural configuration of the silica bilayer is well-understood under UHV conditions from studies employing STM, AFM, transmission electron microscopy, and spectroscopy methods.[28,29,33–37]

We now turn to a comparison of high-resolution LT-UHV-STM and liquid-AFM images of the silica bilayer structure, displayed in Figures 2(a) and 2(b), respectively. A visual comparison of Figs. 2(a) and 2(b) reveals qualitatively similar structures. LT-UHV-STM images generally exhibit protrusions at atomic distances, resolving either individual silicon atoms or individual oxygen atoms, depending on the local tip configuration.[38] In Figure 2(a), the protrusions can be assigned to silicon atoms. They form a network of rings in the two-dimensional plane. Similar ring structures are observed in liquid-AFM, shown in Figure 2(b), where individual ring structures are clearly visible.

In order to characterize the structural configuration for these amorphous materials, we applied pair distance histogram (PDH) plots as a quantitative metric for comparison. Specifically, the characteristic distances associated with the medium-range order of the silica bilayer films are considered,[39] by analyzing the distances between pairs of ring center positions. Ring center positions were determined directly from the images by marking each center manually with vector-based image software. Based on multiple independent ring marking trials, ring center positions determined by this method have an associated precision of approximately 15 pm. To ensure consistency and accuracy, multiple images with high-resolution were analyzed; rings in regions where limited resolution prevented clear ring assignment were not included in the statistics. Approximately 1000 ring center positions were identified and analyzed based on eight images ranging in size from $5 \times 5$ nm$^2$ to $8 \times 8$ nm$^2$ from the liquid-

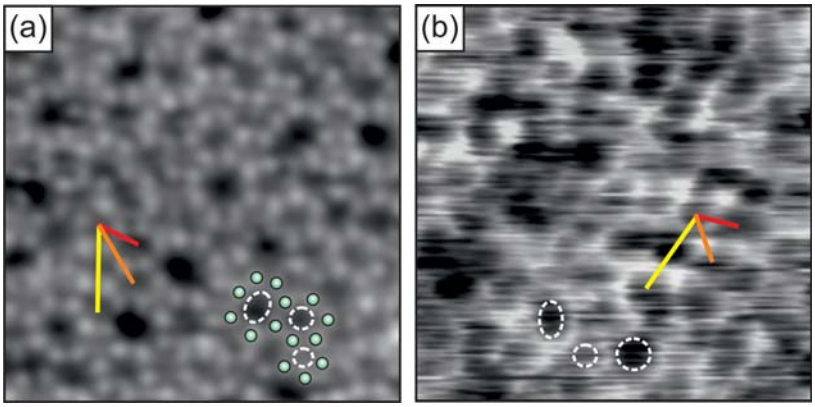


FIG. 2. (a) LT-UHV-STM image of an amorphous silica bilayer film with atomic resolution of silicon atoms. ($5 \times 5\,nm^2$, $I_T = 50\,pA$, $V_s = 2\,V$, $T = 5\,K$). The total height range is 60 pm. The silicon atoms are marked in green for several rings. (b) Liquid-AFM image of an amorphous silica bilayer film shows ring resolution ($5 \times 5\,nm^2$, $f = 337\,kHz$, $A_{imaging} = 0.2\,nm$, $A_{free} = 0.7\,nm$, $k = 26.4\,N/m$, 400 mM aqueous NaCl solution). The total height range is 55 pm. Red, orange, and yellow measurement bars show examples of ring center-center distances for the first three families of ring neighbors identified in the amorphous silica bilayer. Several individual rings are marked in each image.

AFM data set. From the LT-UHV-STM data set, 287 ring centers were identified. A LT-UHV-STM image of a *crystalline* silica film with 71 ring center counts was also analyzed for comparison. The radial distances between all pairs of ring centers were calculated for each image analyzed; radial distances from all images analyzed for a given silica sample and microscopy method were subsequently aggregated for PDH plots.

Figure 3 shows the normalized ring-center PDHs for the amorphous silica structures in liquid (Fig. 3(a)) and UHV (Fig. 3(b)) alongside the PDH for the crystalline silica structure (Fig. 3(c)). A bin size of 0.02 nm is chosen based on empirical optimization. Distance counts are normalized by $4\pi r dr$, where $r$ is the radial distance and d$r$ is the histogram bin size.

The PDHs for the amorphous silica in liquid (Fig. 3(a)) and UHV (Fig. 3(b)) show several peaks associated with the characteristic medium-range order of the amorphous silica bilayer. A polynomial fit of Gaussian curves is utilized to evaluate peak positions and width; peak positions for the first five (first four for the liquid data) are reported in Table I and marked with bold vertical bars on the PDHs in Figure 3. Peak positions are comparable in LT-UHV and liquid measurements. For example, the first peaks for the liquid and UHV data are at $0.53 \pm 0.04$ nm and $0.50 \pm 0.01$ nm, respectively, and second peaks at $0.91 \pm 0.08$ nm and $0.86 \pm 0.02$ nm. Beyond 1.5 nm peaks are increasingly difficult to discern; this is associated with the transition from medium-range order to long-range disorder. As such, we have limited our discussion of PDH peaks to radial distances of less than 2 nm, which both captures the most relevant region for medium-range order and accounts for the finite size limitations introduced by the $5 \times 5\,nm^2$ images that were used for the analysis. In all cases considered within the 2 nm range, peak positions of UHV and liquid data for the amorphous bilayer silica structure agree within the experimental error, though it should be noted that the width of the peaks increases with increasing radial distance. Overall, the LT-UHV-STM PDH peaks are narrower than the liquid-AFM PDH peaks. While the peak widths differ, the quantitative agreement in peak position supports the observed qualitative similarities in the film structures and provides evidence for the robust nature of the silica film when transferred from UHV to liquid environments. Another oxide, $Li_4Ti_5O_{12}(111)$ has also shown similar surface structures between UHV and liquid environments.[40] In contrast, for the rutile $TiO_2(110)$ surface, structural differences between UHV and liquid measurements are observed due to ordering of interfacial water molecules along rows in the presence of bulk liquid.[41] Often UHV surface structures are not stable under ambient conditions due to unsaturated bonds, leading to surface structural changes from hydroxylation reactions.[25,26]

Crystalline bilayer silica films are also examined. The crystalline and amorphous silica bilayer structures differ in the silicon-oxygen-silicon angle, while the stoichiometry remains the same. Peak positions for typical ring-ring center distances from the PDH, plotted in Figure 3(c), are displayed in Table I. These distances are comparable to those in the amorphous phase for the first peaks, but slightly larger at increasing radial distance, especially in the fourth and fifth peak positions. The opposite relationship has been reported for bilayer silica grown on Pd(100), where the first peak in the height-height correlation from images of crystalline silica occurs at a smaller radial distance than that of amorphous silica.[42]

We now turn to a discussion of the physical features of the film structure that give rise to the observed peaks in the ring-center PDHs. In the case of the crystalline lattice, expected peak positions can be derived from an idealized crystalline lattice with a lattice constant of 0.542 nm (based on density functional theory (DFT) calculations) as shown in Figure 3(d).[33] The structure shown in the inset of Figure 3(d) is color-coded to highlight the respective families of neighboring rings, according to the following scheme: A single reference ring is indicated in black and is surrounded by edge sharing nearest-neighbor rings (color-coded in red). Next-nearest-neighbors (orange) are separated from the reference ring by an Si-O-Si bridge, where one silicon atom belongs to the reference ring and the second silicon atom to the next-nearest-neighbor rings. Third-nearest-neighbors (yellow) are separated from the reference ring by the nearest-neighbor (red) rings. In this case, the center of a nearest-neighbor ring lies at the mid-point between

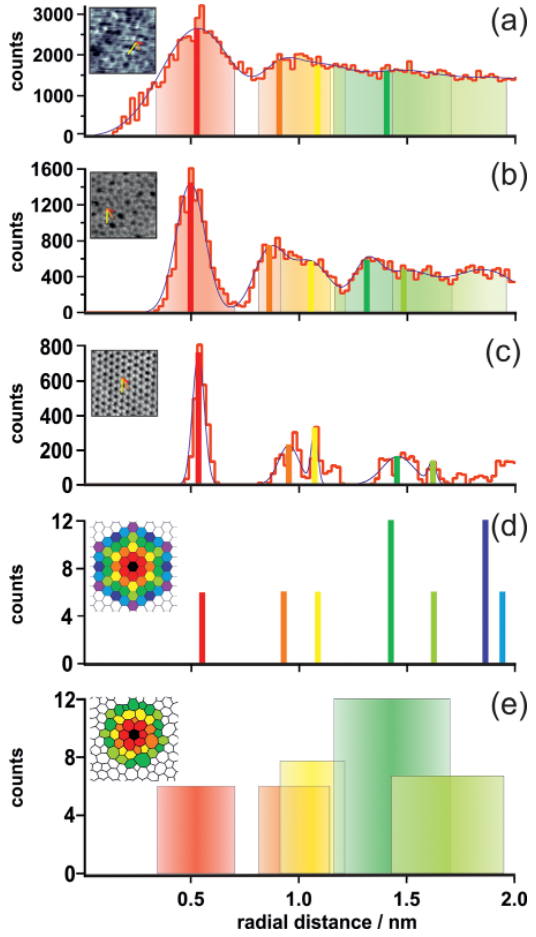


FIG. 3. Normalized pair distance histograms for the ring center-center distances for (a) amorphous silica bilayer measured with liquid-AFM, (b) amorphous silica bilayer measured with LT-UHV-STM, and (c) crystalline silica bilayer measured with LT-UHV-STM. Representative experimental scanning probe microscopy images for each image collection method are shown as insets in each plot. (d) Pair distance histogram for an ideal crystalline model lattice (based on DFT). Inset shows the ideal model lattice with nearest-neighbors, next-nearest-neighbors, etc., color coded around a central reference ring (black). (e) Empirical model for the ranges of values for expected peak positions in pair distance histograms based on different families of ring distances surrounding a reference ring. Inset shows an empirical model developed by direct consideration of a representative UHV microscopy structure for amorphous silica. A black reference ring and is surround by color coded assignment of different ring families.

the centers of the reference ring and third nearest-neighbor ring. Additional fourth, fifth, sixth, and seventh nearest-neighboring rings are colored in a rainbow scheme based on their distance from the central reference ring. The ring-center PDH for the reference ring is shown, without normalization, in Figure 3(d). Histogram bar colors show where distances are associated with nearest-neighbors, next-nearest-neighbors, etc. Comparing the predicted distances shown in Figure 3(d) with the experimental pair correlation function peak fitting shown in Figure 3(c) allows for straightforward interpretation of the physical origin of each of the observed experimental peaks. The maximum deviation between the theoretical and experimental peak value is less than 30 pm (from the fourth peak); all other peaks show agreement between the experimental and theoretical value within the experimental error.

Whereas the crystalline structure enables straightforward assignment of nearest-neighbors and next-nearest-neighbors due to the high symmetry and periodicity in the system, the amorphous system, which lacks lateral periodicity and long range order, does not. For the amorphous structure, an empirical schematic was established based on a representative image of the amorphous bilayer silica structure as measured with LT-UHV-STM (shown in Figure 3(e)). It was analyzed by referencing the crystalline case, rings sharing an edge with the reference ring (indicated in black) are coded in red, rings which are connected by an Si-O-Si bridge to the reference ring are coded in orange, and rings reached from the reference ring by traversing through an edge-sharing ring are indicated in yellow. It should be noted that because rings sizes typically consist of between four and nine silicon atoms, and even rings with the same number of silicon atoms may take on different shapes, ring centers of the bond-sharing rings (nearest-neighbors) around the reference ring do not always lie at the midpoint between the ring centers of the reference ring and yellow-coded rings. A fourth family of rings, coded in dark green, is reached by crossing one Si-O-Si bridge and one ring center starting from the reference ring. A fifth family, coded in light green, is reached by crossing two ring centers from the reference ring. Due to the non-periodic lattice structure, families of rings show a broad range of ring-center-pair distances with respect to the reference ring rather than a single distance. Figure 3(e) shows a plot of the range of distances observed for each set of rings estimated from direct identification of ring families in real-space from experimental LT-UHV-STM images. Edge-sharing neighbors have pair center distances between

TABLE I. Peak positions from Gaussian peak fitting of pair distance histograms. Values from a theoretical model for the crystalline silica hexagonal lattice (based on DFT[33]) and an empirical model of the amorphous silica lattice (developed from experimental LT-UHV-STM structure data) are included for comparison. Peak positions are plotted in Figures 3(a)–3(c), while the theoretical and empirical models are shown in Figures 3(d) and 3(e), respectively.

| | Peak position (nm) | | | | |
|---|---|---|---|---|---|
| | 1st | 2nd | 3rd | 4th | 5th |
| Amorphous silica liquid-AFM PDH | 0.53 ± 0.04 | 0.91 ± 0.08 | 1.09 ± 0.22 | 1.41 ± 0.52 | … |
| Amorphous silica LT-UHV-STM PDH | 0.50 ± 0.01 | 0.86 ± 0.02 | 1.05 ± 0.03 | 1.31 ± 0.02 | 1.48 ± 0.06 |
| Crystalline silica LT-UHV-STM PDH | 0.53 ± 0.01 | 0.95 ± 0.01 | 1.07 ± 0.01 | 1.46 ± 0.02 | 1.62 ± 0.01 |
| Crystalline silica lattice model (DFT) | 0.542 | 0.939 | 1.084 | 1.434 | 1.626 |
| Amorphous silica lattice model (empirical) | 0.34–0.70 | 0.81–1.14 | 0.91–1.21 | … | … |

0.34 and 0.70 nm. Si-O-Si connected orange rings and yellow-coded rings have ranges between 0.81 and 1.14 nm and 0.91 and 1.21 nm, respectively. These ranges overlap with each other, and the features associated with these families of rings in the ring-center PDH will therefore occupy the same region. Ring neighborhood families become increasingly difficult to assign and distinguish with increased distance from the reference ring and peak broadening increases by trend with increasing radial distance.

Comparing the ranges from the schematic analysis with the observed peaks in the pair correlation functions from Figures 3(a) and 3(b) indicates the physical origin of the experimentally determined peaks. The first peak corresponds to edge-sharing neighbors, while the broad second feature is a convolution of the orange and yellow coded neighbor families. In both the liquid data (Fig. 3(a)) and the UHV data (Fig. 3(b)), this feature may be fit with two overlapping Gaussian peaks. The fit Gaussian peaks from Figures 3(a) and 3(b) are consistent with the median values from the empirically derived ring center-center distance ranges for the given neighborhood ring families; curve widths are in good agreement with the estimated peak broadening for the amorphous structure. Clear physical interpretation of the peaks has therefore been established by direct comparison with high resolution structure measurements.

In conclusion, we report high-resolution measurements of amorphous bilayer silica in liquids. A comparison of the interface structure determined from measurements of the amorphous silica bilayer films in UHV and liquid environments shows qualitative and quantitative agreement. This indicates that, contrary to many UHV surface structures, bilayer silica is stable when transferred to ambient conditions. The observed structural preservation of silica under liquid conditions makes it ideally suitable for use in new nanotechnologies. The results of this study demonstrate the promise of liquid-AFM as a methodology for material structure determination at solid-liquid interfaces. This study combined well-defined sample preparation in controlled UHV conditions with imaging under application conditions; this approach may be useful in further materials studies.

The support by the German Science Foundation through CRC 1109 "Understanding of Metal Oxide/Water Systems at the Molecular Scale: Structural Evolution, Interfaces, and Dissolution" as well as by the Fonds der Chemischen Industrie is gratefully acknowledged. Furthermore, K.M.B. thanks the Alexander von Humboldt foundation for funding.

[1]M. A. Brown, A. Goel, and Z. Abbas, Angew. Chem., Int. Ed. **55**, 3790 (2016).
[2]F. Ohnesorge and G. Binnig, Science **260**, 1451 (1993).
[3]F. J. Giessibl, Science **267**, 68 (1995).
[4]S. Morita, F. J. Giessibl, E. Meyer, and R. Wiesendanger, *Noncontact Atomic Force Microscopy* (Springer, 2015), Vol. 3.
[5]D. A. Bonnell, D. N. Basov, M. Bode, U. Diebold, S. V. Kalinin, V. Madhavan, L. Novotny, M. Salmeron, U. D. Schwarz, and P. S. Weiss, Rev. Mod. Phys. **84**, 1343 (2012).
[6]A. Labuda, K. Kobayashi, Y. Miyahara, and P. Grütter, Rev. Sci. Instrum. **83**, 053703 (2012).
[7]D. J. Müller, D. Fotiadis, S. Scheuring, S. A. Müller, and A. Engel, Biophys. J. **76**, 1101 (1999).
[8]S. Rode, N. Oyabu, K. Kobayashi, H. Yamada, and A. Kuehnle, Langmuir **25**, 2850 (2009).
[9]K. Kobayashi, N. Oyabu, K. Kimura, S. Ido, K. Suzuki, T. Imai, K. Tagami, M. Tsukada, and H. Yamada, J. Chem. Phys. **138**, 184704 (2013).
[10]S. Rode, R. Stark, J. Luebbe, L. Troeger, J. Schuette, K. Umeda, K. Kobayashi, H. Yamada, and A. Kuehnle, Rev. Sci. Instrum. **82**, 073703 (2011).
[11]A. Maali, C. Hurth, T. Cohen-Bouhacina, G. Couturier, and J.-P. Aimé, Appl. Phys. Lett. **88**, 163504 (2006).
[12]S. M. R. Akrami, H. Nakayachi, T. Watanabe-Nakayama, H. Asakawa, and T. Fukuma, Nanotechnology **25**, 455701 (2014).
[13]T. Fukuma, K. Kobayashi, K. Matsushige, and H. Yamada, Appl. Phys. Lett. **87**, 034101 (2005).
[14]D. Ebeling and S. D. Solares, Nanotechnology **24**, 135702 (2013).
[15]K. Suzuki, N. Oyabu, K. Kobayashi, K. Matsushige, and H. Yamada, Appl. Phys. Express **4**, 125102 (2011).
[16]N. Kobayashi, S. Itakura, H. Asakawa, and T. Fukuma, J. Phys. Chem. C **117**, 24388 (2013).
[17]T. Ichii, M. Negami, and H. Sugimura, J. Phys. Chem. C **118**, 26803 (2014).
[18]Y. Gan and G. V. Franks, J. Phys. Chem. B **109**, 12474 (2005).
[19]E. T. Herruzo, H. Asakawa, T. Fukuma, and R. Garcia, Nanoscale **5**, 2678 (2013).
[20]J. S. Villarrubia, J. Res. Natl. Inst. Stand. Technol. **102**, 425 (1997).
[21]F. F. Abraham and I. P. Batra, Surf. Sci. Lett. **209**, L125 (1989).
[22]A. K. Geim and I. V. Grigorieva, Nature **499**, 419 (2013).
[23]L. Lichtenstein, M. Heyde, S. Ulrich, N. Nilius, and H.-J. Freund, J. Phys.: Condens. Matter **24**, 354010 (2012).
[24]E. Gao, B. Xie, and Z. Xu, J. Appl. Phys. **119**, 014301 (2016).
[25]F. Ringleb, Y. Fujimori, H.-F. Wang, H. Ariga, E. Carrasco, M. Sterrer, H.-J. Freund, L. Giordano, G. Pacchioni, and J. Goniakowski, J. Phys. Chem. C **115**, 19328 (2011).
[26]F. Ringleb, M. Sterrer, and H.-J. Freund, Appl. Catal., A **474**, 186 (2014).
[27]X. Yu, E. Emmez, Q. Pan, B. Yang, S. Pomp, W. E. Kaden, M. Sterrer, S. Shaikhutdinov, H.-J. Freund, I. Goikoetxea, R. Wlodarczyk, and J. Sauer, Phys. Chem. Chem. Phys. **18**, 3755 (2016).
[28]L. Lichtenstein, C. Buechner, B. Yang, S. Shaikhutdinov, M. Heyde, M. Sierka, R. Wlodarczyk, J. Sauer, and H.-J. Freund, Angew. Chem., Int. Ed. **51**, 404 (2012).
[29]B. Yang, W. E. Kaden, X. Yu, J. A. Boscoboinik, Y. Martynova, L. Lichtenstein, M. Heyde, M. Sterrer, R. Wlodarczyk, M. Sierka, J. Sauer, S. Shaikhutdinov, and H.-J. Freund, Phys. Chem. Chem. Phys. **14**, 11344 (2012).
[30]H.-P. Rust, M. Heyde, and H.-J. Freund, Rev. Sci. Instrum. **77**, 043710 (2006).
[31]M. Heyde, G. H. Simon, H.-P. Rust, and H.-J. Freund, Appl. Phys. Lett. **89**, 263107 (2006).
[32]See supplementary material at http://dx.doi.org/10.1063/1.4949556 for additional microscopy of the silica bilayer film.
[33]D. Löffler, J. J. Uhlrich, M. Baron, B. Yang, X. Yu, L. Lichtenstein, L. Heinke, C. Büchner, M. Heyde, S. Shaikhutdinov, H.-J. Freund, R. Włodarczyk, M. Sierka, and J. Sauer, Phys. Rev. Lett. **105**, 146104 (2010).
[34]C. Buechner, L. Lichtenstein, X. Yu, J. A. Boscoboinik, B. Yang, W. E. Kaden, M. Heyde, S. K. Shaikhutdinov, R. Wlodarczyk, M. Sierka, J. Sauer, and H.-J. Freund, Chem.-Eur. J. **20**, 9176 (2014).
[35]E. I. Altman, J. Götzen, N. Samudrala, and U. D. Schwarz, J. Phys. Chem. C **117**, 26144 (2013).
[36]P. Y. Huang, S. Kurasch, J. S. Alden, A. Shekhawat, A. A. Alemi, P. L. McEuen, J. P. Sethna, U. Kaiser, and D. A. Muller, Science **342**, 224 (2013).
[37]P. Y. Huang, S. Kurasch, A. Srivastava, V. Skakalova, J. Kotakoski, A. V. Krasheninnikov, R. Hovden, Q. Mao, J. C. Meyer, J. Smet, D. A. Muller, and U. Kaiser, Nano Lett. **12**, 1081 (2012).
[38]L. Lichtenstein, M. Heyde, and H.-J. Freund, J. Phys. Chem. C **116**, 20426 (2012).
[39]A. C. Wright, J. Non-Cryst. Solids **179**, 84 (1994).
[40]M. Kitta, M. Kohyama, and H. Onishi, Appl. Phys. Lett. **105**, 111606 (2014).
[41]G. Serrano, B. Bonanni, M. Di Giovannantonio, T. Kosmala, M. Schmid, U. Diebold, A. Di Carlo, J. Cheng, J. VandeVondele, K. Wandelt, and C. Goletti, Adv. Mater. Interfaces **2**, 1500246 (2015).
[42]E. I. Altman and U. D. Schwarz, Adv. Mater. Interfaces **1**, 1400108 (2014).